PAPER

Anisotropic temperature dependence of the electronic band structure in black phosphorus

To cite this article: Lei Zhao *et al* 2025 *Phys. Scr.* **100** 025936

Physica Scripta

PAPER

Anisotropic temperature dependence of the electronic band structure in black phosphorus

RECEIVED
7 November 2024

REVISED
1 January 2025

ACCEPTED FOR PUBLICATION
16 January 2025

PUBLISHED
28 January 2025

Lei Zhao[1,6], **Dandan Shi**[2,6], **Bo Wang**[1], **Yi Liu**[3], **Zhe Sun**[3], **Jingwei Dong**[4,5] and **Zhongwei Chen**[4,5]

[1] School of Science, Northeast Electric Power University, Jilin, 131200, People's Republic of China
[2] Jilin Engineering Normal University, Changchun, 130052, People's Republic of China
[3] National Synchrotron Radiation Laboratory, CAS Center for Excellence in Nanoscience, University of Science and Technology of China, Hefei 230029, People's Republic of China
[4] Power Battery & Systems Research Center, Dalian Institute of Chemical Physics, Chinese Academy of Sciences, Dalian 116023, People's Republic of China
[5] State Key Laboratory of Catalysis, Dalian Institute of Chemical Physics, Chinese Academy of Sciences, Dalian 116023, People's Republic of China
[6] These authors contribute equally to this work.

E-mail: djw1991@dicp.ac.cn

Keywords: black phosphorus, electronic band structure, inter- and intra-layer coupling, electron-phonon scattering, anisotropic temperature dependence

Supplementary material for this article is available online

Abstract

Black phosphorus (BP) has attracted much attention because of its anisotropic layer-dependent optical and electronic structure and ultrahigh carrier mobility. Despite the importance of manipulating the optical and electronic properties of BP by temperature variation, the response of the electronic band structure to temperature and the underlying mechanism which are crucial to understand the related applications haven't been reported yet. Herein, temperature dependence of the electronic band structure of BP has been measured by angle-resolved photoelectron spectroscopy (ARPES) and the band dispersions are quantitatively characterized. While the hole effective mass along k_x (m_x) decreases with temperature, that along k_y (m_y) increases with temperature. We argue that the electronic band dispersion along k_x is decreased because it is dictated by the weakened interlayer and intralayer couplings, and the increase of m_y with temperature is ascribed to the enhanced electron–phonon scattering. This work reports the anisotropic temperature dependence of the electronic band dispersion of BP and reveals the underlying mechanisms, which will expand the knowledge of electronic structure and benefit the understanding of temperature dependent phenomena in this material.

Introduction

Inspired by the advent of experimental monolayer graphene, great efforts have been devoted to the study of two-dimensional (2D) layered semiconductor materials for their potential applications in integrated electronic and optoelectronic devices [1–4]. Compared with the zero band gap graphene [5, 6] and low carrier mobility transition metal dichalcogenides (TMDCs) [7, 8], black phosphorus (BP), an emerging layered semiconductor, has attracted much attention because of its unique optical and electronic properties [9–11]. Retaining the direct band gap, the value is tunable from 0.3 eV in the bulk to 1.5 eV in the monolayer [10, 11]. The on/off ratio and hole-dominated carrier mobility in BP-based field-effect transistors reach 10^5 and 10^3 $cm^2\ V^{-1}s^{-1}$ respectively [12–15]. These properties perfectly overcome the limitations of graphene and TMDCs.

Electronic band structure of BP, which is the foundation to understand the electronic and optoelectronic properties, has been intensively investigated by theoretical calculations [14, 16–18] and angle-resolved photoelectron spectroscopy (ARPES) [19–24]. BP shows anisotropic in plane band structure because of the puckering atomic structure along the x axis [9]. The thickness dependent electronic band dispersion has also been studied as a function of layers [14, 16, 23]. The hole effective mass (m_h), which is a reflection of the band dispersion and an important parameter related to the carrier mobility, can be extracted from the calculated and measured

electronic band. Qiao *et al* predicted the anisotropic layer dependent hole effective mass and high hole mobility [14]. Most recently, Margot *et al* measured the electronic band structure of 2–9 layer BP with micro-focused ARPES, confirming the decrease of m_h with layers along y and the almost independence in x direction [23].

As well as electric fields and surface dipoles, the electronic properties of BP can be modulated by temperature [12, 21, 25–28]. The bandgap of BP is sensitive to temperature [29–31]. Huang *et al* ascribed the abnormal increase of thick BP band gap with temperature to weakened interlayer coupling and the normal decrease of single layer BP band gap with temperature to intensified electron–phonon scattering and thermal expansion [29]. Temperature dependent carrier mobility of BP has also been reported: below 100 K, the carrier mobility remains unaffected and the electron-ionized impurity scattering is proposed to dominate; between 100 K and 300 K, the carrier mobility decrease with temperature, which is attributed to electron–phonon scattering [12].

Because of the layered structure, temperature affects not only the electron–phonon scattering but also the interlayer and intralayer couplings in BP [29]. Therefore, the temperature dependence of the electronic properties becomes complicated as it might arise from electron–phonon scattering and/or interlayer and intralayer couplings. Despite the importance of the electronic band structure in understanding the optical and electric properties of materials, the response of the band dispersion to temperature in BP hasn't been reported yet. In addition, the in-plane band dispersion of BP is anisotropic. It is intriguing to know whether the temperature dependence of the band dispersion is also anisotropic. More important, the decisive role which dictates the evolution of the band structure as a function of temperature needs to be clarified.

In order to address the above important issues in BP, we decoupled the interlayer coupling, intralayer coupling and electron–phonon scattering effects on the electronic band structure in k_x and k_y momentum space by measuring temperature dependent ARPES. The contribution of interlayer coupling, intralayer coupling and electron–phonon scattering were analyzed from temperature dependent ARPES. By fitting m_h and extracting the difference between band peak and valley, the evolution of the electronic band dispersions along the k_x and k_y directions can be monitored quantitatively. Our results suggest that the temperature dependence of m_h along the two high symmetric directions and the underlying mechanism are totally different: m_h along k_x (m_x) is decreased with temperature because it is dictated by the interlayer and intralayer couplings, and m_h along k_y (m_y) increases with temperature which might arise from the electron–phonon scattering. This work presents a systematic investigation of the effect of temperature on the electronic band structure of BP, finds the anisotropic temperature dependence and reveals the underlying mechanisms, which will help to understand the temperature dependent phenomena in BP and provide an example to study the temperature effect in other anisotropic 2D materials.

Experimental and computational details

All ARPES experiments were carried out at the beamline BL13U of the National Synchrotron Radiation Laboratory (NSRL) in Hefei, China. The photon energy of 7.2 eV was used, and the overall energy and momentum resolutions for the ARPES setup were better than 10 meV and 0.2°, respectively. The photoelectrons were collected with a Scienta DA30 analyzer equipped with electrostatic lens allowing Fermi surface mapping without sample rotation. Prior to cleaving, p-type single crystalline BP (Nanjing MKNANO Tech. Co.,Ltd. (www.mukenano.com). thickness: 0.2 mm, lateral dimensions: 1×1 mm^2) is securely mounted onto our sample holder using silver epoxy. When employing silver epoxy, it is essential to heat the sample to 100 °C for approximately 1 h using a heater (model SB 160 by Stuart). This step ensures proper adhesion and curing of the epoxy. Subsequently, a ceramic post is attached, and the entire assembly is enveloped with a graphite coating. This coating is crucial as it provides electrical conductivity to all materials surrounding the cleaved surface, thereby mitigating charging effects that could occur during the photoemission process. To ensure precision and quality at each stage of sample preparation, we utilize a microscope (manufactured by Bresser) for meticulous inspection. In order to obtain a fresh surface for the BP samples in UHV, initially, within the preparation chamber (10 K, 9×10^{-11} Torr, 0 RH), the post holding the sample was gently tapped using a wobble stick. Since the bonding force of epoxy is stronger than the Van der Waals force between the interlayers of a layered material, the crystal can be cleaved by this mechanical force, and a fresh surface results after cleaving. And then the sample was transferred to the measurement chamber (10 K, 7×10^{-11} Torr, 0 RH) for the ARPES experiments. The energy zero in all photoelectron spectra was set at the Fermi level that was referenced to a copper plate in electrical contact with the samples. No charging effect is observed during our measurements.

All DFT calculations were performed using Materials Studio 2017 with the Doml3 software [32, 33]. A generalized gradient approximation was used with the Perdew–Burke–Ernzerhof exchange correlation function [34]. The following configurations were chosen for the geometry optimizations: convergence standards of 10^{-5} Ha on energy, 2×10^{-3} Ha Å on the force, and 5×10^{-3} Å on displacement. The Brillouin zone was sampled using a $4 \times 1 \times 3$ gamma-centered Monkhorst–Pack grid [35–37]. The bands have been shifted to put the maximum of the valence band at 0 eV.

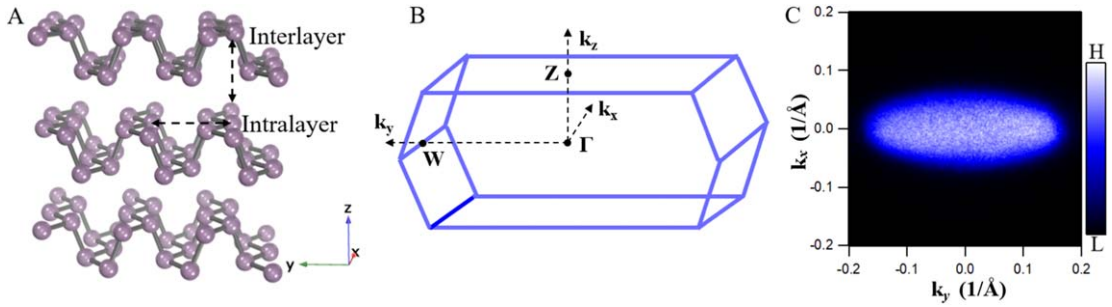

Figure 1. Anisotropic crystal and electronic structures of layered black phosphorus. (A) Layered crystal structure of black phosphorus. (B) Schematic of the 3D Brillouin zone of black phosphorus. (C) Constant-energy contour acquired at the binding energy of 0.15 eV at 10 K. The ellipse shaped contour suggests the anisotropy of the band structure.

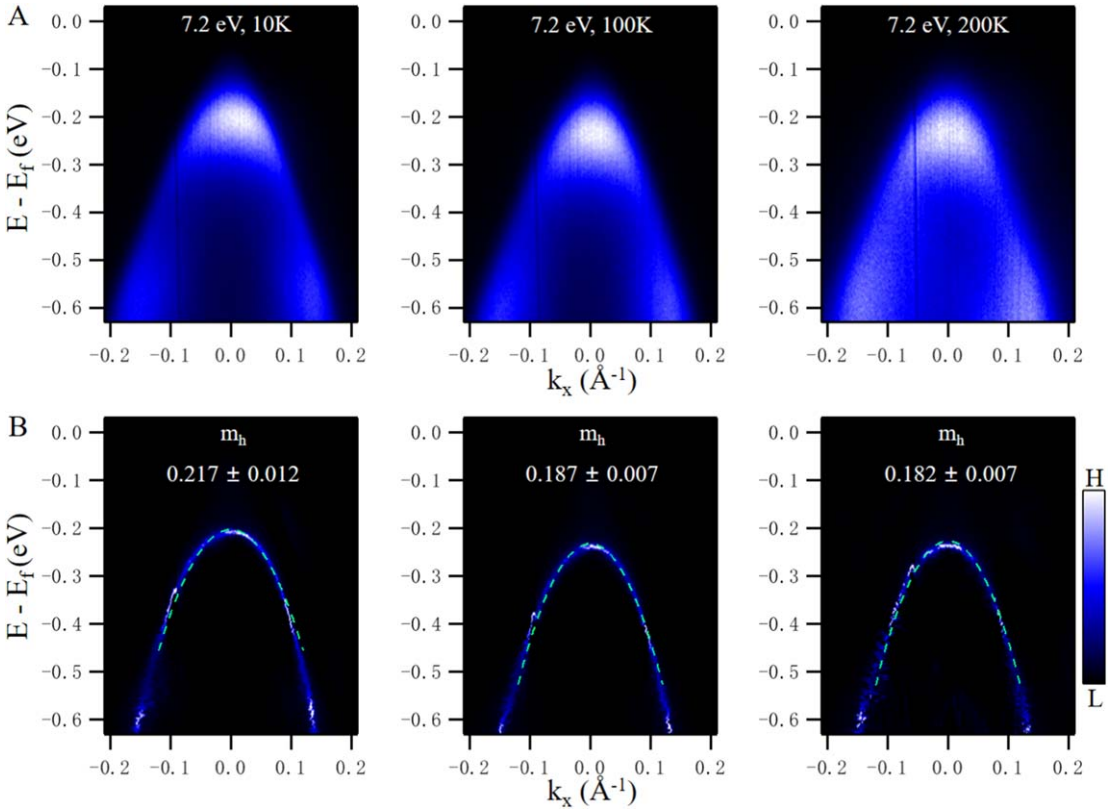

Figure 2. (A) Photoelectron intensity maps recorded along the k_x direction, which show the evolution of the valence band dispersion as functions of sample temperature. (B) Corresponding second-derivative ARPES maps. The green dotted curves represent the modeled dispersion of the valence band. The fitted hole effective mass (m_h) is indicated in the figures. The $m_e$is omitted in the figures for a good visualization.

Results and discussion

Layered BP has a unique crystal structure that is puckered along the *x* direction due to the sp^3 hybridization of phosphorus atoms (figure 1(A)), leading to anisotropic in-plane optoelectronic and electronic properties [9, 17, 22]. Figure 1(B) shows the accompanying Brillouin zone (BZ) of BP primitive cell. According to the elliptic pockets in the constant energy contour at a binding energy of 0.8 eV (figure 1(C)), one can not only discern the two high-symmetry directions of k_x and k_y but also see the anisotropic electronic band dispersion along the two perpendicular in-plane directions.

Figures 2(A) and B show the temperature-dependent photoelectron intensity and corresponding second-derivative maps along the k_x direction. As shown by the green dotted lines in figure 2(B), the fitting curves reproduce the band dispersion along the k_x direction with a high degree of accuracy. The k_x-direction band dispersion is fitted by a parabolic expression,

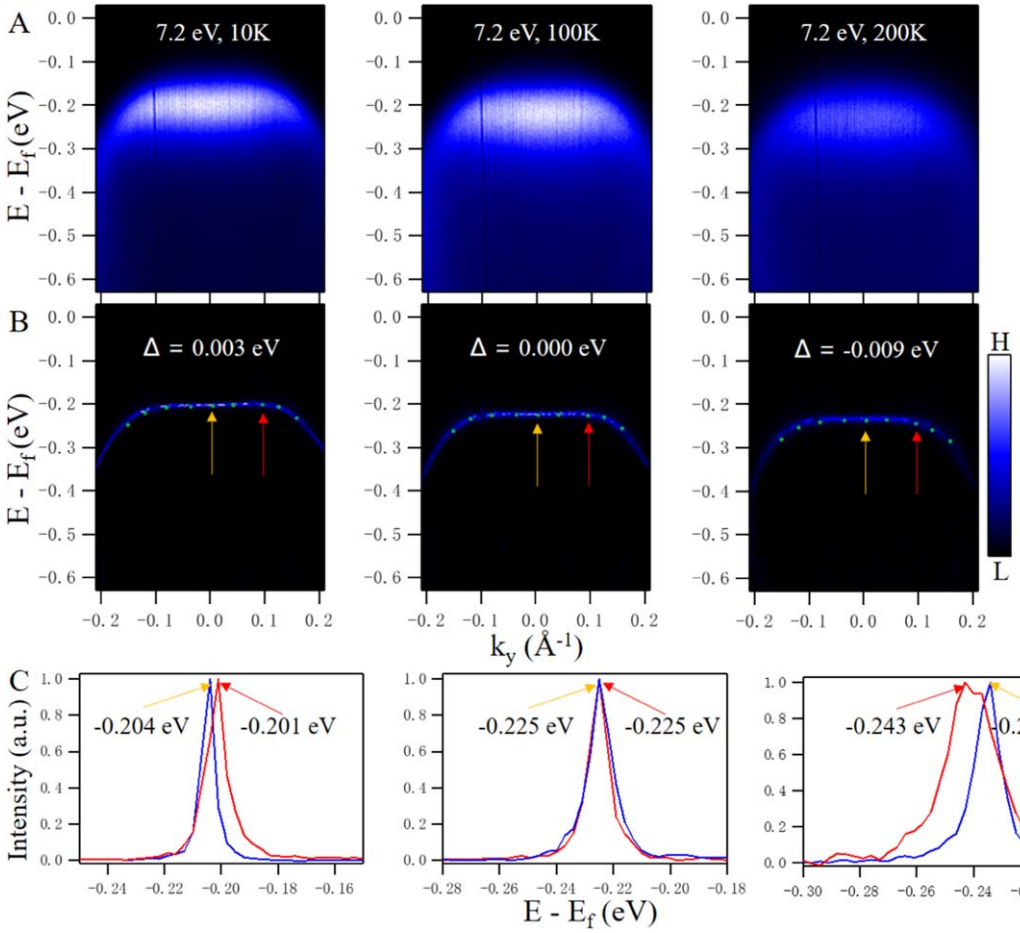

Figure 3. Photoelectron intensity (A) and corresponding second-derivative ARPES (B) maps recorded along the k_y direction, showing the temperature dependence of the valence band dispersion. The orange arrows, red arrows and the green dots represent the binding energies at the momentums of 0 $Å^{-1}$ (band peak or valley) and 0.09 $Å^{-1}$ (band peak or valley), and the valence band maximum at various momentum, respectively. Δ represents the difference of the energies at 0 $Å^{-1}$ and 0.09 $Å^{-1}$. (C) Corresponding energy distribution curves (EDCs) at 0 $Å^{-1}$ (blue curves) and 0.09 $Å^{-1}$ (red curves) at 10 K, 100 K and 200 K, respectively. The orange arrows and red arrows stand for the energy values acquired at 0 $Å^{-1}$ and 0.09 $Å^{-1}$.

$$E = -(\delta + (\hbar k_x)^2/2m_x) \quad (1)$$

where E is energy, δ is a constant, m_x is the hole effective mass, k_x is the wave vector and $\hbar$ is the reduced Planck constant. As shown in figure 2(B), with the temperature changes from 10 to 200 K, the fitted parameters vary from $m_x = 0.217 \pm 0.012\ m_e$ (where m_e is the free electron mass; 10 K), to $m_x = 0.187 \pm 0.007\ m_e$ at 100 K, and finally to $m_x = 0.182 \pm 0.007\ m_e$ at 200 K. The hole effective mass decreases with the temperature within the experimental error.

Identical measurements on the temperature dependence of the valence band along the k_y direction were also performed (figure 3). Figures 3(A) and (B) show the temperature-dependent photoelectron intensity and corresponding second-derivative maps along the k_y direction. As shown in figure 3(B), the green dots, the orange and red arrows represent the valence band maximum at various momentum (band dispersion), the binding energies at the momentums of 0 $Å^{-1}$ (band peak or valley) and 0.09 $Å^{-1}$ (band peak or valley), respectively. The energy distribution curves (EDCs) of the band peak and valley at 10 K, 100 K and 200 K are shown in figure 3(C), and we can extract the energy differences between the band peaks and valleys, respectively. A quantitative analysis shows that the difference between the energies at 0.09 $Å^{-1}$ and 0 $Å^{-1}$ varies from 0.003 eV at 10 K, to 0 eV at 100 K, and finally to −0.009 eV at 200 K. The difference is decreased with the increase of temperature, which indicates the band dispersion is changed to be flat and the hole effective mass is increased.

Next, we discuss the decisive role that dictates the evolution of the band structure as a function of temperature. There is a main feature of the hole effective masses as a function of temperature: the hole effective mass along the k_x direction is decreased upon heating, but that along the k_y direction increase with sample temperature. According to the previous study [29], the distance between two sub-layers decreases by ∼0.4–0.6% when the temperature decreases from 300 K to 10 K, which is comparable to the bulk one. Besides, for samples

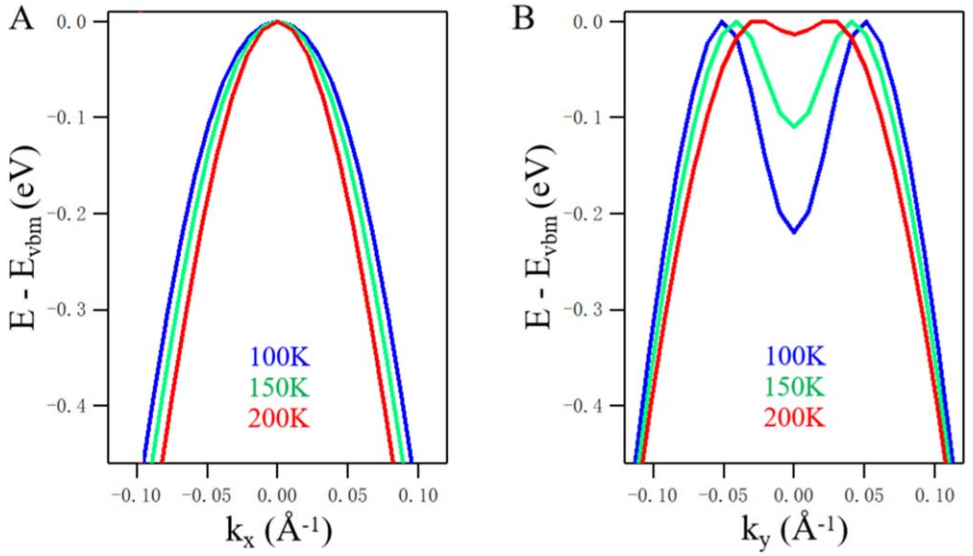

Figure 4. Bands along from slab calculations. The band dispersion at 100 K, 150 K and 200 K are shown with blue, green and red colors, separately.

on BaF_2, the interlayer interaction decreases 10% when the temperature decreases from 10 K to 300 K. Increasing from 10 K to 200 K, both the interlayer and intralayer distances expands, which weakens the interlayer and intralayer interactions of BP and is expected to decrease the hole effective mass. The measured temperature dependence of hole effective mass along the k_x direction, which is consistent with the speculation, indicating that interlayer and intralayer couplings are the factors. Normally, in addition to the interlayer and intralayer couplings, temperature variation may lead to the change of defect density and electron–phonon scattering [12, 29, 38]. BP samples were fabricated at a temperature as high as 860 K. In BP, defects are inevitably introduced during the crystal growth process. Scanning tunneling microscopy (STM) experiments conducted on samples cultivated by 'HQgraphene' have captured atomic-resolution images of stannum (Sn) impurities [39, 40]. Additionally, scanning tunneling spectroscopy (STS) has been employed to investigate vacancies, uncovering significant *p*-doping within the bulk black phosphorus crystal [39]. The STM data indicates an acceptor density of $N \cong 10^{18}$ cm^{-3} [40], which corresponds to the range $0.1 < dN^{1/3} < 1$. Within this regime, the impurities can be conceptualized as a dilute quantum system that forms a narrow energy band [41]. We believe that the concentration of defects doesn't change in the 10–200 K range in the ultra-high-vacuum condition. Therefore, electron-defect scattering will remain the same in this whole temperature range in the current work without introducing additional electronic band dispersion. In terms of the electron–phonon scattering in BP, higher temperature will promote the scattering strength, localize electrons and increase the hole effective mass. Therefore, the electron–phonon scattering is not the positive factor of the decreased hole effective mass along the k_x direction. As illustrated above, along k_y, the hole effective mass is increased upon heating. Thus, enhanced electron–phonon scattering mainly contribute to the increase of m_y rather than the enlarged interlayer and intralayer distances. Anisotropic electron–phonon scattering in different high symmetric directions in BP has been reported [42].We suggest that the weakened interlayer and intralayer couplings contribute to the decrease of m_x, and the enhanced electron–phonon scattering contributes to the increase of m_y upon heating, but future work is needed to quantitatively assess the relative contribution by the Fröhlich model [43]. It should be noted that electron–phonon scattering in polarizable materials is accompanied by the formation of polarons where the charges are surrounded by their induced polarization, which often increase the value of electron/hole effective mass [44]. The polarizability is dependent on the Coulomb interaction between the center charge and the surrounding ions, which is affected by the dielectric constant. In anisotropic BP, the dielectric constant along the armchair direction is higher than that along the zigzag one [45], suggesting the polarization, in other words, the electron–phonon scattering, is weaker along the former. The phonon density of states along the zigzag direction is higher than that along the armchair direction [46]. The stronger Coulomb interaction together with the higher phonon density of states suggests that the electron–phonon scattering in the zigzag direction of BP is more efficient that that in the armchair direction, which has been confirmed by an ultrafast electron diffuse scattering measurement [42]. A theoretical investigation also suggests that the renormalization of hole effective mass of supported monolayer BP is more pronounced along the zigzag direction [47]. These are consistent with the

anisotropic effect of electron–phonon scattering on the electronic band dispersion in our temperature dependent ARPES measurements. Band structure evolution caused by temperature-dependent interlayer coupling has also been found in layered TaS_2 [48]. Phonon-dressed electronic band dispersion has frequently been reported in both two-dimensional and three-dimensional materials [44, 49].

Furthermore, first-principles calculations were performed to reveal the temperature-dependent band structure in BP. Figure 4 shows the calculated band structures of BP along the k_x and k_y directions as a function of temperature. The lattice parameters used to calculate the electronic structure at various temperatures can be extracted from the temperature-dependent x-ray diffraction (XRD) maps (figure S1). As shown in figure 4(A), the band structure near the valence band top demonstrates increased dispersion along the k_x direction with rising temperature. In contrast, the dispersion along the k_y direction is reduced, suggesting that the effective mass m_x decreases while m_y increases upon heating. These calculations agree well with the ARPES experimental results.

Conclusions

In conclusion, valence band structure along k_x and k_y in BP have been investigated by means of photon energy dependent ARPES as a function of temperature, and the response are totally different: the hole effective mass along k_x is decreased upon heating because of the weakened interlayer and intralayer couplings, and that along k_y becomes less dispersive with increasing temperature which is mainly ascribed to the enhanced electron–phonon scattering. The finding and understanding of anisotropic temperature dependence of the electronic band structure in BP will benefit the manipulation of the optical and electronic properties through temperature in this material and other anisotropic 2D materials.

Acknowledgments

This work is supported by the Natural Science Foundation of China (Grant No. 22409194), the Energy Revolution S&T Program of Yulin Innovation Institute of Clean Energy, (Grant No. YlCE E411060316), the Strategic Priority Research Program of the Chinese Academy of Sciences (Grant No. XDB0600000, XDB0600200) and Natural Science Foundation of Liaoning Province (Grant No.2024BSBA27).

Conflicts of interest/competing interest

The authors declared that there is no conflict ofinterest in this manuscript.

Data availability statement

All data that support the findings of this study are included within the article (and any supplementary files).

Associated content

Supplementary data

The supplementary data is shown as the following:

Single-crystal XRD maps;

Band dispersion along the k_z direction.

ORCID iDs

Jingwei Dong https://orcid.org/0009-0007-8521-7549
Zhongwei Chen https://orcid.org/0009-0009-9941-3377

References

[1] Bonaccorso F, Colombo L, Yu G, Stoller M, Tozzini V, Ferrari A C, Ruoff R S and Pellegrini V 2015 Graphene, related two-dimensional crystals, and hybrid systems for energy conversion and storage *Science* **347** 1246501
[2] Wang Q H, Kalantar-Zadeh K, Kis A, Coleman J N and Strano M S 2012 Electronics and optoelectronics of two-dimensional transition metal dichalcogenides *Nat. Nanotechnol.* **7** 699
[3] Liu Y, Duan X, Shin H-J, Park S, Huang Y and Duan X 2021 Promises and prospects of two-dimensional transistors *Nature* **591** 43
[4] Tan C *et al* 2023 2D fin field-effect transistors integrated with epitaxial high-k gate oxide *Nature* **616** 66
[5] Novoselov K S, Geim A K, Morozov S V, Jiang D, Katsnelson M I, Grigorieva I V, Dubonos S and Firsov A A 2005 Two-dimensional gas of massless Dirac fermions in graphene *Nature* **438** 197
[6] Geim A K and Novoselov K S 2007 The rise of graphene *Nat. Mater.* **6** 183
[7] Manzeli S, Ovchinnikov D, Pasquier D, Yazyev O V and Kis A 2017 2D transition metal dichalcogenides *Nat. Rev. Mater.* **2** 1
[8] Radisavljevic B, Radenovic A, Brivio J, Giacometti V and Kis A 2011 Single-layer MoS2 transistors *Nat. Nanotech.* **6** 147
[9] Buscema M, Groenendijk D J, Blanter S I, Steele G A, Van Der Zant H S and Castellanos-Gomez A 2014 Fast and broadband photoresponse of few-layer black phosphorus field-effect transistors *Nano Lett.* **14** 3347
[10] Liu H, Neal A T, Zhu Z, Luo Z, Xu X, Tománek D and Ye P D 2014 Phosphorene: an unexplored 2D semiconductor with a high hole mobility *ACS nano* **8** 4033
[11] Xia F, Wang H and Jia Y 2014 Rediscovering black phosphorus as an anisotropic layered material for optoelectronics and electronics *Nat. Commun.* **5** 4458
[12] Li L, Yu Y, Ye G J, Ge Q, Ou X, Wu H, Feng D, Chen X H and Zhang Y 2014 Black phosphorus field-effect transistors *Nat. Nanotech.* **9** 372
[13] Doganov R A, O'farrell E C, Koenig S P, Yeo Y, Ziletti A, Carvalho A, Campbell D K, Coker D F, Watanabe K and Taniguchi T 2015 Transport properties of pristine few-layer black phosphorus by van der waals passivation in an inert atmosphere *Nat. Commun.* **6** 6647
[14] Qiao J, Kong X, Hu Z X, Yang F and Ji W 2014 High-mobility transport anisotropy and linear dichroism in few-layer black phosphorus *Nat. Commun.* **5** 4475
[15] Ahmed F, Kim Y D, Yang Z, He P, Hwang E, Yang H, Hone J and Yoo W J 2018 Impact ionization by hot carriers in a black phosphorus field effect transistor *Nat. Commun.* **9** 3414
[16] Tran V, Soklaski R, Liang Y and Yang L 2014 Layer-controlled band gap and anisotropic excitons in few-layer black phosphorus *Phys. Rev.* B **89** 235319
[17] Ling X, Huang S, Hasdeo E H, Liang L, Parkin W M, Tatsumi Y, Nugraha A R, Puretzky A A, Das P M and Sumpter B G 2016 Anisotropic electron-photon and electron-phonon interactions in black phosphorus *Nano lett.* **16** 2260
[18] Takao Y and M A 1981 Electronic structure of black phosphorus: tight binding approach *Physica* B **105** 93
[19] Takahashi T, Tokailin H, Suzuki S, Sagawa T and Shirotani I 1984 Highly-angle-resolved ultraviolet photoemission study of a black-phosphorus single crystal *Phys. Rev.* B **29** 1105
[20] Han C, Yao M, Bai X, Miao L, Zhu F, Guan D, Wang S, Gao C, Liu C and Qian D 2014 Electronic structure of black phosphorus studied by angle-resolved photoemission spectroscopy *Phys. Rev.* B **90** 085101
[21] Kim J, Baik S S, Ryu S H, Sohn Y, Park S, Park B-G, Denlinger J, Yi Y, Choi H J and Kim K S 2015 Observation of tunable band gap and anisotropic Dirac semimetal state in black phosphorus *Science* **349** 723
[22] Chen Z, Dong J, Papalazarou E, Marsi M, Giorgetti C, Zhang Z, Tian B, Rueff J P, Taleb-Ibrahimi A and Perfetti L 2019 Band gap renormalization, carrier multiplication, and stark broadening in photoexcited black phosphorus *Nano Lett.* **19** 488
[23] Margot F, Lisi S, Cucchi I, Cappelli E, Hunter A, Gutiérrez-Lezama I, Ma K, von Rohr F, Berthod C and Petocchi F 2023 Electronic structure of few-layer black phosphorus from μ-ARPES *Nano Lett.* **23** 6433
[24] Zhou S *et al* 2023 Pseudospin-selective floquet band engineering in black phosphorus *Nature* **614** 75
[25] Liu Y, Qiu Z, Carvalho A, Bao Y, Xu H, Tan S J, Liu W, Castro Neto A, Loh K P and Lu J 2017 Gate-tunable giant stark effect in few-layer black phosphorus *Nano Lett.* **17** 1970
[26] Chen Z, Dong J, Giorgetti C, Papalazarou E, Marsi M, Zhang Z, Tian B, Ma Q, Cheng Y and Rueff J-P 2020 Spectroscopy of buried states in black phosphorus with surface doping *2D Mater.* **7** 035027
[27] Kim S-W, Jung H, Kim H-J, Choi J-H, Wei S-H and Cho J-H 2017 Microscopic mechanism of the tunable band gap in potassium-doped few-layer black phosphorus *Phys. Rev.* B **96** 075416
[28] Deng B, Tran V, Xie Y, Jiang H, Li C, Guo Q, Wang X, Tian H, Koester S J and Wang H 2017 Efficient electrical control of thin-film black phosphorus bandgap *Nat. Commun.* **8** 14474
[29] Huang S *et al* 2020 From anomalous to normal: temperature dependence of the band gap in two-dimensional black phosphorus *Phys. Rev. Lett.* **125** 156802
[30] Chen C, Chen F, Chen X, Deng B, Eng B, Jung D, Guo Q, Yuan S, Watanabe K and Taniguchi T 2019 Bright mid-infrared photoluminescence from thin-film black phosphorus *Nano lett.* **19** 1488
[31] Villegas C E, Rocha A and Marini A 2016 Anomalous temperature dependence of the band gap in black phosphorus *Nano Lett.* **16** 5095
[32] Zhang K, Wang Q, Wang B, Xu Y, Ma X and Li Z 2019 A DFT study on CO methanation over the activated basal plane from a strained two-dimensional nano-MoS_2 *Appl. Surf. Sci.* **479** 360
[33] Gui X, Zhou Q, Peng S, Xu L and Zeng W 2020 Adsorption behavior of Rh -doped MoS_2 monolayer towards SO_2, SOF_2, SO_2F_2 based on DFT study *Physica E Low Dimens. Syst. Nanostruct.* **122** 114224
[34] Perdew J P, Burke K and Ernzerhof M 1997 Generalized gradient approximation made simple *Phys. Rev. Lett.* **78** 1396
[35] Monkhorst H J and Pack J D 1976 Special points for Brillouin-zone integrations *Phys. Rev.* B **13** 5188
[36] Rao K V K, Naidu S V N and Iyengar L 1970 Thermal expansion of rutile and anatase *J. Am. Ceram. Soc.* **53** 124
[37] Mott N F and Stoneham A M 1977 Lifetime of electrons, holes and excitons before self-trapping *Solid State Phys.* **10** 3391
[38] Li J V and Levi D H 2011 Determining the defect density of states by temperature derivative admittance spectroscopy *J. Appl. Phys.* **109**
[39] Kiraly B, Hauptmann N, Rudenko A N, Katsnelson M I and Khajetoorians A A 2017 Probing single vacancies in black phosphorus at the atomic level *Nano Lett.* **17** 3607
[40] Qiu Z *et al* 2017 Resolving the spatial structures of bound hole states in black phosphorus *Nano Lett.* **17** 6935
[41] Shklovskii B and Efros A L 1984 *Electronic Properties of Doped Semiconductors* (Springer: Heidelberg)
[42] Seiler H *et al* 2021 Accessing the anisotropic nonthermal phonon populations in black phosphorus *Nano Lett.* **21** 6171
[43] Fröhlich H 1954 Electrons in lattice fields *Adv. Phys.* **3** 325
[44] Puppin M *et al* 2020 Evidence of large polarons in photoemission band mapping of the perovskite semiconductor $CsPbBr_3$ *Phys. Rev. Lett.* **124** 206402

[45] Nagahama T, Kobayashi M, Akahama Y, Endo S and Narita S-i 1985 Optical determination of dielectric constant in black phosphorus *J. Phys. Soc. Japan* **54** 2096
[46] Chaves A, Ji W, Maassen J, Dumitrica T and Low T 2017 Theoretical overview of black phosphorus *in 2D Materials: Properties and Devices* (Cambridge University Press) 2017, 381
[47] Mogulkoc A, Mogulkoc Y, Rudenko A and Katsnelson M 2016 Polaronic effects in monolayer black phosphorus on polar substrates *Phys. Rev.* B **93** 085417
[48] Wang Y, Yao W, Xin Z, Han T, Wang Z, Chen L, Cai C, Li Y and Zhang Y 2020 Band insulator to mott insulator transition in 1 T-TaS_2 *Nat. Commun.* **11** 4215
[49] Mazzola F, Wells J W, Yakimova R, Ulstrup S, Miwa J A, Balog R, Bianchi M, Leandersson M, Adell J and Hofmann P 2013 Kinks in the σ band of graphene induced by electron-phonon coupling *Phys. Rev. Lett.* **111** 216806